Article

Explanation of the Unusual Temperature Dependence of the Atmospherically Important OH + HS → HO + HS Reaction and Prediction of the Rate Constant at Combustion Temperatures

Benjamin A. Ellingson, and Donald G. Truhlar

J. Am. Chem. Soc., **2007**, 129 (42), 12765-12771• DOI: 10.1021/ja072538b • Publication Date (Web): 02 October 2007

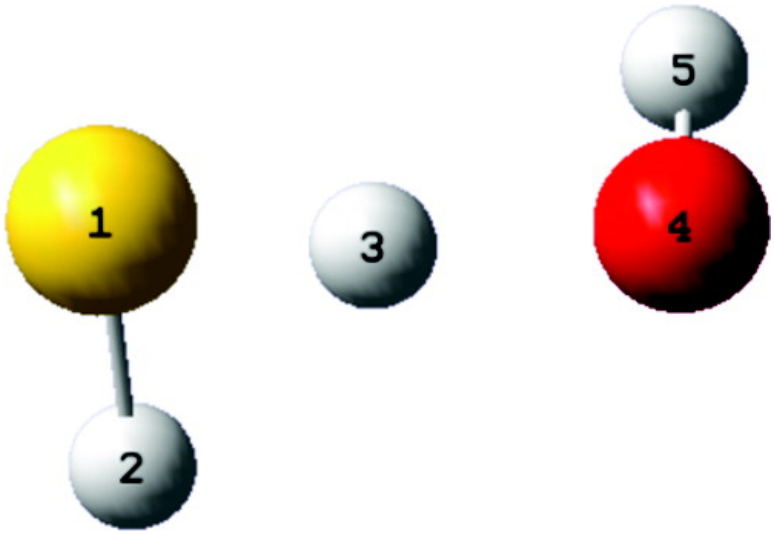

More About This Article

Additional resources and features associated with this article are available within the HTML version:

- Supporting Information
- Links to the 3 articles that cite this article, as of the time of this article download
- Access to high resolution figures
- Links to articles and content related to this article
- Copyright permission to reproduce figures and/or text from this article

View the Full Text HTML

J|A|C|S
ARTICLES
Published on Web 10/02/2007

Explanation of the Unusual Temperature Dependence of the Atmospherically Important OH + H_2S → H_2O + HS Reaction and Prediction of the Rate Constant at Combustion Temperatures

Benjamin A. Ellingson and Donald G. Truhlar*

Contribution from the Department of Chemistry and Supercomputing Institute, University of Minnesota, 207 Pleasant Street SE, Minneapolis, Minnesota 55455-0431

Received April 11, 2007; E-mail: truhlar@umn.edu

Abstract: Rate constants for the OH + H_2S → H_2O + HS reaction, which is important for both atmospheric chemistry and combustion, are calculated by direct dynamics with the M06-2X density functional using the MG3S basis set. Energetics are compared to high-level MCG3/3//MC-QCISD/3 wave function theory and to results obtained by other density functionals. We employ canonical variational transition-state theory with multidimensional tunneling contributions and scaled generalized normal-mode frequencies evaluated in redundant curvilinear coordinates with anharmonicity included in the torsion. The transition state has a quantum mechanically distinguishable, nonsuperimposable mirror image that corresponds to a separate classical reaction path; the effect of the multiple paths is examined through use of a symmetry number and by torsional methods. Calculations with the reference-potential Pitzer−Gwinn treatment of the torsional mode agree with experiment, within experimental scatter, and predict a striking temperature dependence of the activation energy, increasing from −0.1 kcal/mol at 200 K to 0.2, 1.0, 3.4, and 9.8 kcal/mol at 300, 500, 1000, and 2400 K. The unusual temperature dependence arises from a dynamical bottleneck at an energy below reactants, following an addition complex on the reaction path with a classical binding energy of 4.4 kcal/mol. As a way to check the mechanism, kinetic isotope effects of the OH + D_2S and OD + D_2S reactions have been predicted.

Introduction

The reaction of OH with H_2S is a key step in the primary chain of the explosive oxidation of H_2S[1] and in H_2S ignition,[2] and it also plays an important role in atmospheric chemistry. The flux of sulfur in the atmosphere is composed primarily of dimethyl sulfide and hydrogen sulfide,[3] with hydrogen sulfide accounting for about 2% of total gaseous sulfur and a higher percentage (less than 10%) of natural sulfur. Hydrogen sulfide is primarily oxidized by OH with a recommended rate constant of $4.5 \pm 1.0 \times 10^{-12}$ cm^3 molecule^{-1} sec^{-1} at 298 K.[3] A significant amount of experimental data[3−10] is available for this reaction, and rate constants show an unusual temperature dependence that has so far eluded theoretical explanation. It is important to develop general theories of the temperature dependence of rate constants because they often need to be extrapolated for atmospheric applications to lower temperatures than where they have been measured and for combustion applications to higher temperatures than where they have been measured.

Even without considering the unusual temperature dependence, the OH + H_2S → H_2O + SH reaction has proved to be a very difficult system to model theoretically. Previous theoretical studies[11] have yielded rate constants that are much lower than experimental results at room temperature and have too steep of an Arrhenius slope. The correct barrier height for the reaction is an essential element of a valid model, as is a correct application of the forward symmetry number and the treatment of the multiple classical reaction paths associated with the hindered rotation of the transition state. The present work addresses these concerns in the context of direct dynamics calculations employing density functional theory (DFT) as the electronic-structure method to characterize the implicit potential-energy surface. The barrier height and energy of reaction are also compared to high-level wave function theory (WFT). The reaction is studied in the atmospherically important temperature

(1) (a) Barnard, J. A.; Bardsley, J. N. *Flame and Combustion*; Chapman and Hall: London, 1985. (b) Glassman, I. *Combustion*; Academic: Orlando, FL, 1987.
(2) (a) Frenklach, M.; Lee, J. H.; White, J. N.; Gradiner, W. C. J. *Combust. Flame* **1981**, *41*, 1. (b) Gargurevich, I. A. *Ind. Eng. Chem. Res.* **2005**, *44*, 7706.
(3) Tyndall, G. S.; Ravishankara, A. R. *Int. J. Chem. Kinet.* **1991**, *23*, 483.
(4) Westenberg, A. A.; DeHaas, N. *J. Chem. Phys.* **1973**, *59*, 6685.
(5) Perry, R. A.; Atkinson, R.; Pitts, J. N. J. *J. Chem. Phys.* **1976**, *64*, 3237.
(6) Leu, M.-T.; Smith, R. H. *J. Phys. Chem.* **1982**, *86*, 73.
(7) Michael, J. V.; Nava, D. F.; Brobst, W. D.; Borkowski, R. P.; Stief, L. J. *J. Phys. Chem.* **1982**, *86*, 81.
(8) Lin, Y.-H.; Wang, N.-S.; Lee, Y.-P. *Int. J. Chem. Kinet.* **1985**, *17*, 1201.
(9) Lafage, C.; Pauwels, J.-F.; Carlier, M.; Devolder, P. *J. Chem. Soc. Faraday Trans. 2* **1987**, *83*, 731.
(10) See also (a) Wine, P. H.; Kreutter, N. M.; Gump, C. A.; Ravishankara, A. R. *J. Phys. Chem.* **1981**, *85*, 2660. (b) Lin, C. L. *Int. J. Chem. Kinet.* **1982**, *14*, 593.
(11) (a) Wilson, C.; Hirst, D. M. *J. Chem. Soc., Faraday Trans.* **1994**, *90*, 3051. (b) Mousavipour, S. H.; Namdar-Ghanbari, M. A.; Sadeghian, L. *J. Phys. Chem. A* **2003**, *107*, 3752.

10.1021/ja072538b CCC: $37.00

range of 200−300 K and also up to the top of the upper range of temperatures of interest for combustion, in particular up to 2400 K. In addition we predict two kinetic isotope effects that have been suggested as mechanistic probes by experimentalists.

Computational Details

Electronic Structure Methods and Energetics. The rate constants determined in the present work are calculated with four levels of DFT, namely the MPW1K/MG3S, BB1K/MG3S, MPWB1K/MG3S, and M06-2X/MG3S levels of theory, where MG3S is a basis set explained in the next paragraph. MPW1K,[12] BB1K,[13] and MPWB1K[14] are one-parameter hybrid density functionals for which the percentage of Hartree−Fock (HF) exchange has been parametrized for the calculation of accurate kinetics data (in particular barrier heights and energies of reaction). Calculations with these methods were carried out using Gaussian 03.[15] M06-2X[16] is a hybrid meta density functional with high HF exchange; it represents a refinement of the M05-2X[17] functional and shows excellent performance for both barrier heights and noncovalent interactions in a large validation suite,[16] which makes it the recommended density functional method for kinetics, especially when one must also consider entrance-valley van der Waals complexes in the mechanism. Calculations employing the M06-2X method were carried out using Gaussian 03-MN-GFM,[18] which is a locally modified module adding new density functional capability to Gaussian 03.[15]

All DFT methods are calculated with the MG3S basis set,[19] which is equivalent to MG3[20] without the diffuse basis functions on hydrogens. (MG3 is also called G3LargeMP2.[21]) MG3S is an improved[21] version of the 6-311+G(3d2f,2df,2p)[19,21] triple-split Gaussian basis set, and we have found in previous work[22] that it is a good basis set for barrier height calculations.

The forward barrier height and energy of reaction were calculated with the above four density functionals and also by the MC-QCISD/3[23] and MCG3/3//MC-QCISD/3[20,23] multicoefficient correlation methods, where MCG3/3//MC-QCISD/3 signifies a single-point energy calculation performed with MCG3/3 at the MC-QCISD/3 optimized geometry. MC-QCISD/3 and MCG3/3 are high-level multicoefficient correlation methods in which individual WFT components are combined to extrapolate to a more accurate result. These methods were calculated using MULTILEVEL, version 4.2.[24]

The calculated barrier heights and energies of reaction are listed in Table 1.

Rate Constant Calculations. All rate constant calculations were performed with POLYRATE, version 9.6,[25] and the DFT methods were interfaced with POLYRATE via GAUSSRATE, version 9.6.[26]

Table 1. Barrier Heights ($V^{\ddagger}$ and Energy of Reaction (ΔE) for the $OH + H_2S \rightarrow H_2O + SH$ Reaction[a]

method	$V^{\ddagger}$ (kcal/mol)	ΔE (kcal/mol)	S–H(3) distance (Å)	O–H(3) distance (Å)
MCG3/3//MC-QCISD/3	0.41	−31.4		
MC-QCISD/3	0.82	−30.9	1.403	1.479
M06-2X	−0.24	−29.5	1.394	1.497
MPWB1K	0.75	−26.9	1.398	1.456
BB1K	0.36	−27.1	1.396	1.469
MPW1K	0.64	−26.6	1.399	1.453

[a] The values in this table are zero-point exclusive, that is, the classical barrier height and classical equilibrium energy of reaction.

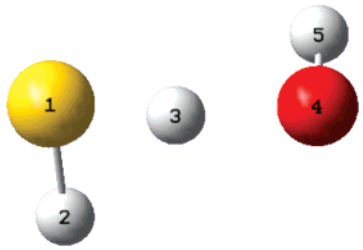

Figure 1. Picture of the saddle point with numbered atoms calculated at the M06-2X level of theory.

Table 2. Stretches, Bends, and Torsions for the Redundant Internal Coordinates

stretches	bends	torsions
2−1	2−1−3	2−1−3−4
1−3	1−3−4	1−3−4−5
3−4	3−4−5	2−1−4−5
4−5	2−1−4	
1−4	1−4−5	

The minimum energy path (MEP) was calculated with a step size of 0.00265 Å in mass-scaled coordinates with a scaling mass of 1 amu, and a Hessian was calculated every 10 steps. The electronically excited $^2\Pi_{1/2}$ state with excitation energy of 140 cm^{-1} was included when calculating the reactant electronic partition functions of OH. All other species are assumed to have significant population only in their ground electronic states.

The rate constants are calculated using variational transition state theory with multidimensional tunneling.[27,28] Specifically, canonical variational transition state theory[29,30] (CVT) is used with a transmission coefficient κ^{SCT} calculated by the small curvature tunneling[31] approximation; the resulting rate constant is labeled (CVT/SCT). Calculations at the MPW1K level show that microcanonically optimized multidimensional tunneling[32] (μOMT) results agree with SCT results; therefore, large-curvature tunneling[28,32,33] is negligible for this reaction and was not included.

A picture of the transition state at the M06-2X level with labeled atoms is shown in Figure 1. The values of the coordinates listed in Table 2 are tabulated for the transition state optimized at the M06-2X level in Table 3. Frequencies along the reaction path were calculated

(12) Lynch, B. J.; Fast, P. L.; Harris, M.; Truhlar, D. G. *J. Phys. Chem. A* **2000**, *104*, 4811.
(13) Zhao, Y.; Lynch, B. J.; Truhlar, D. G. *J. Phys. Chem. A* **2004**, *108*, 2715.
(14) Zhao, Y.; Truhlar, D. G. *J. Phys. Chem. A* **2004**, *108*, 6908.
(15) Frisch, M. J.; et al. *Gaussian 03*, revision C.02; Gaussian, Inc: Wallingford, CT, 2004.
(16) Zhao, Y.; Truhlar, D. G. *Theor. Chem. Acc.*, published online, Jul 12, 2007, http://dx.doi.org/10.1007/s00214-007-0310-x.
(17) Zhao, Y.; Schultz, N. E.; Truhlar, D. G. *J. Chem. Theory Comput.* **2006**, *2*, 364.
(18) Zhao, Y.; Truhlar Donald, G. *MN-GFM: Minnesota Gaussian Functional Module*, version 3.0; University of Minnesota: Minneapolis, MN, 2006.
(19) Lynch, B. J.; Zhao, Y.; Truhlar, D. G. *J. Phys. Chem. A* **2003**, *107*, 1384.
(20) Fast, P. L.; Sanchez, M. L.; Truhlar, D. G. *Chem. Phys. Lett.* **1999**, *306*, 407.
(21) Curtiss, L. A.; Redfern, P. C.; Raghavachari, K.; Rassolov, V. A.; Pople, J. A. *J. Chem. Phys.* **1999**, *110*, 4703.
(22) Zheng, J.; Zhao, Y.; Truhlar, D. G. *J. Chem. Theory Comput.* **2007**, *3*, 593.
(23) Lynch, B. J.; Truhlar, D. G. *J. Phys. Chem. A* **2003**, *107*, 3898.
(24) Zhao, Y.; Rodgers, J. M.; Lynch, B. J.; Gonzalez-Garcia, N.; Fast, P. L.; Pu, J.; Ellingson, B. A.; Truhlar, D. G. *MULTILEVEL*, version 4.2; University of Minnesota: Minneapolis, MN, 2006.
(25) Corchado, J. C.; et al. *POLYRATE*, version 9.6; Univeristy of Minnesota: Minneapolis, MN, 2007.
(26) Corchado, J. C.; Chuang, Y.-Y.; Coitino, E. L.; Ellingson, B. A.; Truhlar, D. G. *GAUSSRATE*, version 9.6; University of Minnesota: Minneapolis, MN, 2007.
(27) Truhlar, D. G.; Isaacson, A. D.; Garret, B. C. In *Theory of Chemical Reaction Dynamics*; Baer, M., Ed.; CRC Press: Boca Raton, FL, 1985; Vol. 3, p 65.
(28) Fernandez-Ramos, A.; Ellingson, B. A.; Garrett, B. C.; Truhlar, D. G. In *Reviews in Computational Chemistry*; Lipkowitz, K. B., Cundari, T. R., Eds.; Wiley-VCH: Hoboken, NJ, 2007; Vol. 23, p 125.
(29) Truhlar, D. G.; Garrett, B. C. *Acc. Chem. Res.* **1980**, *13*, 440.
(30) Garrett, B. C.; Truhlar, D. G. *J. Chem. Phys.* **1979**, *70*, 1593.
(31) Liu, Y.-P.; Lynch, G. C.; Truong, T. N.; Lu, D.-h.; Truhlar, D. G.; Garrett, B. C. *J. Am. Chem. Soc.* **1993**, *115*, 2408.
(32) Liu, Y.-P.; Lu, D.-h.; Gonzalez-Lafont, A.; Truhlar, D. G.; Garrett, B. C. *J. Am. Chem. Soc.* **1993**, *115*, 7806.
(33) Garrett, B. C.; Truhlar, D. G.; Wagner, A. F.; Dunning, T. H., Jr. *J. Chem. Phys.* **1983**, *78*, 4400.

Table 3. Values of the Coordinates Listed in Table 2 for the M06-2X Optimized Transition State

stretches (Å)	bends (deg)	torsions (deg)
1.337	92.1	70.8
1.394	137.5	37.9
1.497	104.1	107.8
0.970	85.2	
2.712	88.5	

with the RODS algorithm,[34] where RODS denotes "reorientation of the dividing surface," and all frequencies (both along the reaction path and in computing the 0 K enthalpies of association of the reaction complexes) were scaled using the frequency scaling factors found at http://comp.chem.umn.edu/database/freq_scale.htm. In particular, MPW1K frequencies are scaled by 0.9581,[13] BB1K frequencies are scaled by 0.9590,[13] MPWB1K frequencies are scaled by 0.9567,[14] and M06-2X frequencies are scaled by 0.982.[16]

The Symmetry Number and Hindered Internal Rotation. The symmetry number for the OH + $H_2S \rightarrow H_2O$ + SH reaction based on rotational symmetry numbers is two, arising from a rotational symmetry number of two for H2S and one for both OH and the transition state.[35] Additionally, the mirror image of the transition state is nonsuperimposable and thus quantum mechanically distinguishable, and it is not accounted for in the rotational symmetry numbers. Treating the mirror image as a separate elementary reaction would yield an additional factor of 2, such that the total forward rate would be accounted for with a reaction-path symmetry number of four.[35] However, the question remains as to whether the classical reaction paths are sufficiently independent such that they may be treated as separate elementary reactions by means of a symmetry number.

The question of independence may be examined by treating the two reaction paths as a hindered internal rotation of a single system. The hindered internal rotation, or torsion, can be modeled as the −OH group rotating about an axis that is collinear with the breaking S−H bond. The effective internal moment of inertia, *I*, corresponding to this internal rotation is evaluated using the method of Pitzer and Gwinn.[36−38]

The harmonic oscillator (HO) partition function[39] for each vibrational mode *m* is given by

$$Q_m^{\mathrm{HO}} = \frac{\exp(-\beta\hbar\omega_m/2)}{1-\exp(-\beta\hbar\omega_m)} \tag{1}$$

where ω_m is the harmonic vibrational frequency of mode *m*. The HS−H−OH transition state involves multiple distinguishable minima due to its nonsuperimposable mirror image. For an internal rotation involving multiple distinguishable minima, such as the hydrogen peroxide molecule,[38] all distinguishable minima can be accounted for at the harmonic level of approximation using the multiconformer HO (MC−HO) treatment,[40,41] which yields

$$Q_m^{\mathrm{MC-HO}} = \sum_{j=1}^{P} \frac{\exp(-\beta(U_j + \hbar\omega_{mj}/2))}{1-\exp(-\beta\hbar\omega_{mj})} \tag{2}$$

where *P* is the number of distinguishable minima, ω_{mj} is the harmonic frequency at minimum *j* of torsional mode *m*, and U_j is the energy of well *j* of this mode relative to the lowest well of this mode. Because this system involves modeling mirror images with identical properties, $U_1 = U_2 = 0$ and $\omega_{m1} = \omega_{m2}$, which means that $Q_m^{\mathrm{MC-HO}} = 2Q_m^{\mathrm{HO}}$.

Therefore, treating the system as a whole with a symmetry number of 2 and the MC−HO treatment is equivalent to treating the nonsuperimposable paths separately with a symmetry number of 4 and the simple HO treatment. Some torsional methods involve a harmonic oscillator component. Since the torsional methods are modeling the system as a whole, it is vital that the MC−HO treatment is used for this component.

Three torsional methods are evaluated along the MEP. For the first method,[42] labeled MN, the partition function for the torsional mode is estimated via

$$Q_{\mathrm{tor}}^{\mathrm{MN}} = Q_{\mathrm{tor}}^{\mathrm{MC-HO}} \tanh\left(\frac{Q_{\mathrm{tor}}^{\mathrm{FR}}}{Q_{\mathrm{tor}}^{\mathrm{I}}}\right) \tag{3}$$

where $Q_{\mathrm{tor}}^{\mathrm{MC-HO}}$ is given by eq 2 and $Q_{\mathrm{tor}}^{\mathrm{I}}$ and $Q_{\mathrm{tor}}^{\mathrm{FR}}$ are intended to model the partition function at intermediate temperatures and in the high-temperature, free-internal-rotator limit, respectively. The intermediate-temperature partition function, $Q_{\mathrm{tor}}^{\mathrm{I}}$, is evaluated by taking the high-temperature limit of eq 2,

$$Q_{\mathrm{tor}}^{\mathrm{I}} = \sum_{j=1}^{P} \frac{\exp(-\beta U_j)}{\hbar\beta\omega_{\mathrm{tor}j}} \tag{4}$$

where $\hbar$ is Planck's constant divided by 2π. The free-internal-rotator approximation, $Q_{\mathrm{tor}}^{\mathrm{FR}}$, to the torsional partition function is given by

$$Q_{\mathrm{tor}}^{\mathrm{FR}} = \frac{(2\pi IkT)^{1/2}}{\hbar\sigma} \tag{5}$$

where σ is the internal rotational symmetry number, which is unity because the wells are distinguishable.

The second method is a Pitzer−Gwinn-type method, labeled as RPG,[36,38] based on a reference potential of a simple cosine curve. The RPG torsional partition function is given by

$$Q_{\mathrm{tor}}^{\mathrm{RPG}} = \left[\frac{Q_{\mathrm{tor}}^{\mathrm{MC-HO}}}{Q_{\mathrm{tor}}^{\mathrm{I}}}\right] Q_{\mathrm{tor}}^{\mathrm{FR}} \exp(-\beta W/2) I_0(\beta W/2) \tag{6}$$

where *W* is the barrier height to internal rotation and $I_0(\beta W/2)$ is a modified Bessel function. When the torsional potential is represented by a simple cosine curve, the moment of inertia, the torsional frequency, and the barrier height are related by

$$\omega_{\mathrm{tor}} = \sigma\left(\frac{W}{2I}\right)^{1/2} \tag{7}$$

The frequency that most resembles the torsional motion is the second-lowest real frequency at the saddle point, which is approximately 275 cm^{-1}. (The lowest frequency, which is 172−205 cm^{-1}, depending on the electronic structure method, corresponds primarily to an S−H−O bend.) Because reliable frequencies and moments of inertia are available along the MEP, eq 7 is used to calculate the barrier height from the torsional frequency and the effective internal moment of inertia.

(34) Villa, J.; Truhlar, D. G. *Theor. Chem. Acc.* **1997**, *97*, 317.
(35) Fernandez-Ramos, A.; Ellingson B. A.; Meana-Pandea, R.; Marques, J. M. C.; Truhlar Donald, G. *Theor. Chem. Acc*., published online Jul 11, 2007, http://dx.doi.org/s00214-007-0328-0.
(36) Pitzer, K. S.; Gwinn, W. D. *J. Chem. Phys.* **1942**, *10*, 428.
(37) Pitzer, K. S. *J. Chem. Phys.* **1946**, *14*, 239.
(38) Ellingson, B. A.; Lynch, V. A.; Mielke, S. L.; Truhlar, D. G. *J. Chem. Phys.* **2006**, *125*, 084305/1.
(39) Wilson, E. B.; Decius, J. C.; Cross, P. C. *Molecular Vibrations*; McGraw-Hill Book Company: New York, 1955.
(40) Lynch, V. A.; Mielke, S. L.; Truhlar, D. G. *J. Phys. Chem. A* **2005**, *109*, 10092.
(41) Chuang, Y.-Y.; Truhlar, D. G. *J. Chem. Phys.* **2000**, *112*, 1221.
(42) Truhlar, D. G. *J. Comput. Chem.* **1991**, *12*, 266.

Table 4. Torsional Data Using M06-2X at the Saddle Point (300 K)

ω_{tor} (cm^{-1})		274.5
W (kcal/mol)		2.649
I (au)		5398.6
Q_{tor}	FR	5.6768
	HO	1.4149
	I	1.5193
	MC−HO	1.4149
	MN	1.4133
	RPG	1.5310
	AS	1.5270

Table 5. M06-2X Forward Rate Constants (in cm^3 $molecule^{-1}$ s^{-1}) with the Torsional Mode Treated by the MC−HO, MN, RPG, and AS Approximations

T (K)	MC–HO	MN	RPG	AS
200	4.19×10^{-12}	4.19×10^{-12}	4.38×10^{-12}	4.37×10^{-12}
250	3.98×10^{-12}	3.98×10^{-12}	4.20×10^{-12}	4.19×10^{-12}
300	3.95×10^{-12}	3.95×10^{-12}	4.23×10^{-12}	4.22×10^{-12}
350	4.14×10^{-12}	4.13×10^{-12}	4.50×10^{-12}	4.50×10^{-12}
400	4.41×10^{-12}	4.40×10^{-12}	4.87×10^{-12}	4.87×10^{-12}
600	6.29×10^{-12}	6.24×10^{-12}	7.25×10^{-12}	7.28×10^{-12}
1000	1.34×10^{-11}	1.30×10^{-11}	1.57×10^{-11}	1.57×10^{-11}
1500	2.31×10^{-11}	2.16×10^{-11}	2.61×10^{-11}	2.62×10^{-11}
2400	6.48×10^{-11}	5.65×10^{-11}	6.66×10^{-11}	6.70×10^{-11}

The third method is a parametrized version of the RPG method by Ayala and Schlegel,[43] labeled AS. The AS torsional partition function is

$$Q^{AS} = \frac{1 + P_2 \exp[-\beta W/2]}{1 + P_1 \exp[-\beta W/2]} Q^{RPG} \quad (8)$$

where P_1 and P_2 are fifth order polynomial functions[38,43] of $1/Q_{tor}^{FR}$ and $\beta W/2$, respectively.

A comparison of the torsional partition functions calculated by these methods is given in Table 4. The first three quantities are those that are the same for all of the methods, and the remaining quantities are various approximations to the partition function for the torsional mode. Additionally, rate constants calculated with M06-2X with each of the final four methods have been listed in Table 5 and plotted in Figure 2. The MN method was designed to interpolate between the MC−HO partition function and Q_{tor}^{FR}, but it is not between them for this transition state. The RPG and AS methods yield very similar results. The torsional methods indicate that the MC−HO approximation gives reasonable results, which means that treating the total forward reaction with a symmetry number of 4 and the simple HO approximation would not be a poor approximation. However, the RPG and AS methods show that there is a torsional effect, so the RPG method has been chosen to be used when calculating rate constants. The RPG method was chosen over the AS method because the parametrization does not appear to yield any significant benefit in the present case.

Results and Discussion

Recent studies have provided estimates of reliabilities of the various methods in Table 1 for barrier heights of hydrogen-atom transfer reactions; these studies[16,22] yielded mean unsigned errors of 0.8 kcal/mol for MCG3/3, 0.9 kcal/mol for MC-QCISD/3, 1.1 kcal/mol for M06-2X and BB1K, 1.3 kcal/mol for MPWB1K, and 1.4 kcal/mol for MPW1K. Thus none of the methods is reliable to the few tenths of a kcal/mol that would be required for truly quantitative predictions. For the present reaction, of the four density functionals considered, M06-2X has the best agreement with high-level WFT for the energy of reaction (Table 1), although not for the barrier height. This is encouraging because M06-2X also showed the best general performance on previous validation tests.[16,22] The best judge of accuracy for the present reaction is, however, comparison to experiment. Rate constants for the DFT direct dynamics calculations are listed in Table 6 and plotted in Figure 3; the M06-2X density functional best reproduces the experimental results. M06-2X is the only level of theory that yields a negative classical barrier height; however, the maximum in the generalized free energy of activation profile[44] is +0.06 kcal/mol.

Thus the explanation of the unusual temperature dependence of the rate constant is a negative barrier that becomes a dynamical bottleneck because of the tightening of vibrations transverse to the reaction path. A similar situation is well-known

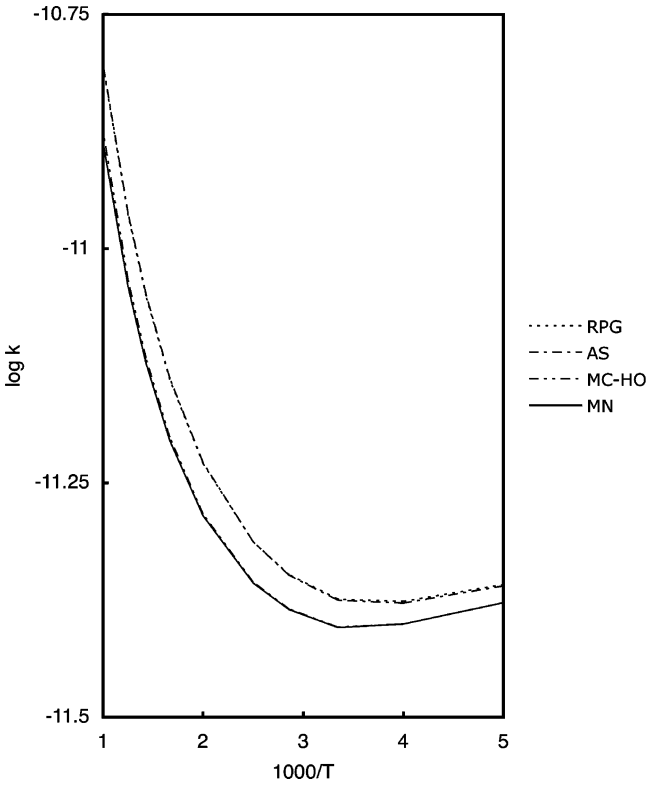

Figure 2. Rate constants (cm^3 $molecule^{-1}$ s^{-1}) calculated with M06-2X level of theory with the MC−HO, MN, RPG, and AS torsional methods. The logarithms in this figure are to the base 10. The curves are listed in the legend in the same order (top-to-bottom) that they occur in the graph, but two of the curves are hard to see because the RPG and AS curves are almost on top of one another, as are the MC-HO and MN curves.

Table 6. Forward Rate Constants (in cm^3 $Molecule^{-1}$ Sec^{-1}) for M06-2X, MPWB1K, BB1K, and MPW1K with the Torsional Mode Treated at the RPG Level

T (K)	M06-2X	MPWB1K	BB1K	MPW1K
200	4.38×10^{-12}	2.25×10^{-12}	3.23×10^{-12}	1.81×10^{-12}
250	4.20×10^{-12}	2.51×10^{-12}	3.38×10^{-12}	1.94×10^{-12}
300	4.23×10^{-12}	2.91×10^{-12}	3.68×10^{-12}	2.21×10^{-12}
350	4.50×10^{-12}	3.43×10^{-12}	4.09×10^{-12}	2.58×10^{-12}
400	4.87×10^{-12}	3.97×10^{-12}	3.95×10^{-12}	2.98×10^{-12}
600	7.25×10^{-12}	6.10×10^{-12}	6.26×10^{-12}	5.30×10^{-12}
1000	1.57×10^{-11}	1.53×10^{-11}	1.44×10^{-11}	1.34×10^{-11}
1500	2.61×10^{-11}	3.07×10^{-11}	2.80×10^{-11}	3.06×10^{-11}
2400	6.66×10^{-11}	8.54×10^{-11}	7.86×10^{-11}	8.37×10^{-11}

(43) Ayala, P. Y.; Schlegel, H. B. *J. Chem. Phys.* **1998**, *108*, 2314.

(44) Garrett, B. C.; Truhlar, D. G.; Grev, R. S.; Magnuson, A. W. *J. Phys. Chem.* **1980**, *84*, 1730.

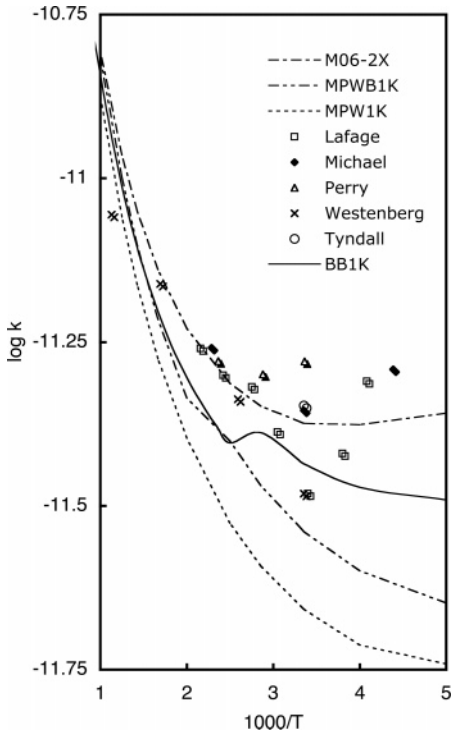

Figure 3. Calculated and experimental rate constants (cm^3 $molecule^{-1}$ s^{-1}). The logarithms in this figure are to the base 10.

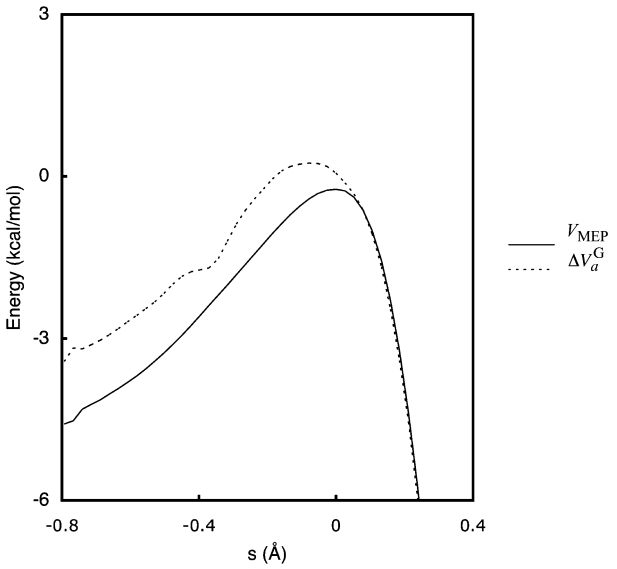

Figure 4. $V_{MEP}(s)$ and $\Delta V_a^G(s)$ curves (kcal/mol) calculated by M06-2X.

to occur in many gas-phase S_N2 reactions.[45,46] The effect can already be understood by simply adding the local zero-point energy, ZPE(*s*), to the potential energy $V_{MEP}(s)$ along the MEP as a function of signed distance *s* (in the mass-scaled coordinate system[47]) from the saddle point, as illustrated in Figure 4. The ground-state vibrationally adiabatic potential, $V_a^G(s)$, is defined as[44,48]

$$V_a^G(s) = V_{MEP}(s) + ZPE(s) \quad (9)$$

and the figure shows the relative ground-state vibrationally adiabatic potential, $\Delta V_a^G(s)$, which is defined for a bimolecular reaction as $V_a^G(s)$ minus the zero-point energy for reactants. For a bimolecular reaction, except for symmetry factors, this relative curve corresponds to the generalized free energy of activation at 0 K.[49] In the discussion below, it will be important that the vibrationally adiabatic potential curve also serves as the effective barrier for tunneling.

Table 7. Energy of Activation in kcal/mol for M06-2X with the Torsional Mode Treated at the RPG Level

T (K)	E_a
200	−0.12
300	0.16
400	0.56
500	1.01
600	1.48
800	2.46
1000	3.44
1500	5.69
2400	9.80

The unusual phenomenon of the rate constant decreasing more than the error bars as the temperature increases in the atmospherically important temperature range up to 300 K has been observed by Leu et al.,[6] Lin et al.,[8] and Lafage et al.[9] The M06-2X level is the only level of theory tested that agrees with this observed feature of the rate constants. This provides a strong indication that M06-2X yields a qualitatively correct picture of the reaction. A similar phenomenon has been found[50] for the OH + $CH_3SH \rightarrow H_2O$ + CH_3S reaction, which has a more negative classical barrier than OH + H_2S and a negative maximum in the ΔV_a^G (*s*) function due to the stabilizing effect of the methyl group.

The unusual temperature dependence of the rate constant also leads to an unusual dependence of the Arrhenius activation energy, defined by[51]

$$E_a = -R \frac{d \ln k}{d(1/T)} \quad (10)$$

Our results for the Arrhenius activation energy as a function of temperature are given in Table 7. The activation energy increases by almost 10 kcal/mol over the temperature range studied. Strong temperature dependences of the Arrhenius activation energy have also been observed for other reactions,[52,53] and this should make one cautious about equating the Arrhenius activation energy to the barrier height, as is often done.

It has been suggested by Tyndall and Ravishankara[3] that the kinetic isotope effects (KIEs) of the OH + D_2S and OD + D_2S reactions with respect to the OH + H_2S reaction would be informative in deducing the reaction mechanism. Specifically, they indicated that experimental measurements of these two KIEs would clarify the involvement, if any, of an addition complex of OH and H_2S. KIEs calculated at the M06-2X level with the RPG method for the torsion are given in Table 8. If

(45) Olmstead, W. N.; Brauman, J. I. *J. Am. Chem. Soc.* **1977**, *99*, 4219.
(46) Hu, W.-P.; Truhlar, D. G. *J. Am. Chem. Soc.* **1995**, *117*, 10726.
(47) Isaacson, A. D.; Truhlar, D. G. *J. Chem. Phys.* **1982**, *76*, 1380.
(48) Garrett, B. C.; Truhlar, D. G. *J. Chem. Phys.* **1980**, *72*, 3560.
(49) Garrett, B. C.; Truhlar, D. G. *J. Am. Chem. Soc.* **1979**, *101*, 4534.
(50) Masgrau, L.; Gonzalez-Lafont, A.; Lluch, J. M. *J. Phys. Chem. A* **2003**, *107*, 4490.
(51) Truhlar, D. G. *J. Chem. Educ.* **1978**, *55*, 309.
(52) Truhlar, D. G.; Gray, J. C. *Chem. Phys. Lett.* **1978**, *57*, 93.
(53) (a) Blais, N. C.; Truhlar, D. G.; Garrett, G. C. *J. Phys. Chem.* **1981**, *85*, 1094. (b) Blais, N. C.; Truhlar, D. G.; Garrett, B. C. *J. Chem. Phys.* **1982**, *76*, 2768. (c) Garrett, B. C.; Truhlar, D. G.; Bowman, J. M.; Wagner, A. F.; Robie, D.; Arepalli, S.; Presser, N.; Gordon, R. J. *J. Am. Chem. Soc.* **1986**, *108*, 3515.

Table 8. Kinetic Isotope Effects for the Forward Rate Constants Calculated Using M06-2X with the Torsional Mode Treated at the RPG Level

T (K)	H2S-OH/ D2S-OH	H2S-OH/ D2S-OD
200	1.64	2.98
250	1.70	3.10
298	1.73	3.15
300	1.73	3.15
350	1.77	3.24
400	1.81	3.31
500	1.85	3.41
600	1.88	3.47
700	1.89	3.50
800	1.90	3.50
1000	1.89	3.46
1500	1.46	2.61
2400	1.41	2.44

Table 9. Values of the Coordinates Listed in Table 2 for the M06-2X Optimized Addition Complex

stretches (Å)	bends (deg)	torsions (deg)
1.336	92.5	−70.6
1.336	79.4	−51.0
2.660	103.5	−130.6
0.969	72.4	
2.749	85.0	

experimental measurements are carried out and found to be in agreement with the values calculated here, that would provide a further verification of the assumptions of the present treatment. One key assumption of treating the reaction by transition state theory as a bimolecular reaction is that that all reactants states are in local equilibrium.[54,55] This is equivalent to assuming that an OH + H_2S addition complex, if present at a significant concentration, is in equilibrium with reactants.

We can use theory to say more about the presence of an addition complex because the M06-2X/MG3S method is quite accurate for noncovalent interactions.[16] Optimization of an addition complex yields a well that is 4.8 kcal/mol deep with structure similar to the addition complex of $CH_3S(OH)CH_3$ determined by González-García et al.[56] The single-point counterpoise correction[57] lowers this to 4.4 kcal/mol. The dynamics calculations do not include counterpoise corrections. The distance from the sulfur atom to the hydrogen atom in OH is 2.83 Å, and the O−H and S−O distances are 0.97 and 2.75 Å with an H−S−O bond angle of 75.1°. The full geometry of this HS(OH)H addition complex is given in Table 9. A hydrogen-bonded structure of the form considered by Wang et al.[58] for $H_2S(HO)$ and by Uchimaru et al.[59] for $H_2O(HO)$ was found to be higher in energy than the addition complex by 1.3 kcal/mol (without counterpoise corrections).

Including zero-point energy lowers the M06-2X/MG3S binding energy of the HS(OH)H complex from the classical equilibrium value of −4.83 kcal/mol to the 0 K enthalpy of association value of −0.87 kcal/mol; in contrast the M06-2X/MG3S energy of the HS(HO)H complex is lowered from −3.50 to −2.95 kcal/mol. Thus the zero-point energy contributions switch which of the two complexes is energetically preferred.

The MPW1K MEP has been followed toward reactants, and it was found that the HS(OH)H addition complex is the one that occurs on the MEP; and it occurs at a reaction coordinate value of about −3 Å.

It has been emphasized in previous work[60,61] that accurate modeling of reactive potential-energy surfaces requires accurate modeling of prebarrier van der Waals wells to ensure that the shape of the barrier is correct in the region where the interaction potential crosses from negative (at larger distances) to positive (as one approaches the barrier). This is even more important when one has a negative barrier height. The M06-2X density functional is especially well suited to modeling this kind of reaction because it has been well validated both for attractive noncovalent interactions in van der Waals complexes and for reactive barrier heights, so it can treat the competition of attractive and repulsive forces more reliably than previous functionals.

The effective barrier for tunneling in the SCT approximation is the adiabatic ground-state potential-energy curve $V_a^G(s)$ defined in eq 9 above. When zero-point energy is added, the M06-2X/MG3S barrier height at the saddle point is raised from −0.24 to +0.06 kcal/mol. However, as shown in Figure 4, the effective barrier to tunneling is even larger at a position earlier than the saddle point. The maximum of the vibrationally adiabatic ground-state potential-energy curve occurs at $s = -0.073$ Å, where it has a value 0.25 kcal/mol higher than the value at reactants.

Before commenting on the magnitude of tunneling effect, it is useful to recall the formulation of a consistent transmission coefficient[28,29,44] for CVT. The CVT/SCT rate constant may be written as

$$k^{\mathrm{CVT/SCT}} = \kappa^{\mathrm{CVT/CAG}} \kappa^{\mathrm{SCT}} k^{\mathrm{CVT}} \qquad (11)$$

where $\kappa^{\mathrm{CVT/CAG}}$ is the classical adiabatic ground-state (CAG) transmission coefficient, and κ^{SCT} accounts for the quantum effects on the reaction coordinate, namely tunneling and nonclassical reflection from $V_a^G(s)$. The first factor, $\kappa^{\mathrm{CVT/CAG}}$, is less than unity because the maximum of $V_a^G(s)$ does not occur at the CVT variational transition state; thus, the limit of the SCT transmission coefficient corresponding to the reaction-coordinate motion being classical is not unity. This accounts for reflection by the part of the effective barrier that is higher than the effective barrier value at the CVT variational transition state; the true quantum effect is given by the second factor.[29,44] In early papers on VTST, we often labeled κ^{T} (where T denotes the tunneling method, e.g., T is SCT for the present paper or VAG in some early papers) as $\kappa^{\mathrm{T/VAG}}$, and we labeled the product of $\kappa^{\mathrm{CVT/CAG}}$ and κ^{T} as $\kappa^{\mathrm{CVT/T}}$. Very often, $\kappa^{\mathrm{CVT/CAG}}$ is close to unity, and, as reviewed elsewhere,[28] in more recent papers—to simplify the acronyms because high-precision acronyms are longer and seem to discourage some readers—we usually label $\kappa^{\mathrm{CVT/T}}$ as κ^{T} since it is clear to specialists (from

(54) Boyd, R. K. *Chem. Rev.* **1977**, *77*, 93.
(55) Fernandez-Ramos, A.; Miller, J. A.; Klippenstein, S. J.; Truhlar, D. G. *Chem. Rev.* **2006**, *106*, 4518.
(56) González-García, N.; González-Lafont, À.; Lluch, J. M. *J. Comput. Chem.* **2005**, *26*, 569.
(57) Boys, S. F.; Bernardi, F. *Mol. Phys.* **1970**, *19*, 553.
(58) Wang, C.; Zhang, G.; Wang, Z.; Li, Q.; Zhang, Y. *THEOCHEM* **2005**, *731*, 187.
(59) Uchimaru, T.; Chandra, A.; Tsuzuki, S.; Sugie, M.; Sekiya, A. *J. Comput. Chem.* **2003**, *24*, 1538.
(60) Truhlar, D. G.; Horowitz, C. J. *J. Chem. Phys.* **1978**, *68*, 2466.
(61) Masgrau, L.; Gonzalez-Lafont, A.; Lluch, J. M. *J. Comput. Chem.* **1999**, *20*, 1685.
(62) Rai, S. N.; Truhlar, D. G. *J. Chem. Phys.* **1983**, *79*, 6046.

Table 10. Temperature Dependence[a]

	k: OH + H_2S			KIE: [OH + H_2S]/[OH + D_2S]		
T(K)	TST	CVT	CVT/SCT	TST	CVT	CVT/SCT
300	5.23	4.17	4.23	2.14	1.71	1.73
800	12.1	11.2	10.9	2.11	1.97	1.90
2400	89.4	77.8	66.6	1.89	1.64	1.41

[a] Rate constants in units of 10^{-12} cm^3 $molecule^{-1}$ s^{-1}.

the context) that we mean $\kappa^{CVT/T}$ (since we always use the consistent treatment). Here, however, $\kappa^{CVT/CAG}$ is significantly less than unity (it ranges from 0.98 at 200 K to 0.86 at 2300 K; the actual values are tabulated in Supporting Information), and so one must keep the precise distinctions in mind. (Another simplification that we sometimes make when the distinction is not important is to refer to κ^T as the tunneling factor, although actually it includes both tunneling and nonclassical reflection, and it should more precisely be called the effect of quantum mechanical reaction-coordinate motion. For reactions with high effective barriers to tunneling, tunneling is much more important than nonclassical reflection, but this is not the case for small effective barriers to tunneling.)

For the present reaction, quantum effects on the reaction-coordinate motion are small, which is to be expected for a reaction with a negative classical barrier, although these effects are not zero because there is an effective barrier for tunneling when (as in eq 9) transverse zero-point energy requirements have been added along the reaction path (as shown in Figure 4). In particular, κ^{SCT} (the second factor on the right side of eq 10, that is, $\kappa^{SCT/VAG}$) is 1.17 at 200 K and 1.07 at 300 K, and it is only 1.001 at 2400 K.

The variational effect, k^{TST}/k^{CVT}, where TST denotes conventional transition state theory so that the ratio shows how much the rate is decreased by optimizing the location of the transition state, is 1.46 at 200 K and 1.25 at 300 K, and it falls to 1.15 at 2400 K. This is a reasonably small effect at high temperature, but it is not at all negligible at 200 K. The observation that variational effects are small at high temperature is interesting because they are sometimes much larger for low-barrier reactions at high temperature.[55]

Isotopic substitution affects the tunneling and variational effects. The maximum in $\Delta V_a^G(s)$ occurs at $s = -0.07$ Å for OH + H_2S, at $s = -0.0003$ Å for OH + D_2S, and at $s = -0.0002$ Å for OD + D_2S, corresponding to a negligible variational effect for both of the deuterated systems. Tunneling plays less of a role for the deuterated systems than for OH + H_2S, with κ^{SCT}equal to only 1.01 even at 200 K. Therefore, for the deuterated systems, the rate constant is almost the same with conventional TST as with CVT or CVT/SCT. But this is not true for the perprotio system, as illustrated in Table 10. Table 10 shows that the decrease in the isotope effect from 800 to 2400 K is mainly a variational effect. The canonical variational transition state moves in at high temperature, which is by now a well-known effect[62] for early transition states; it is associated with the tightening of the bends and torsion involving new bonds. In the present case the four lowest-frequency modes of the generalized transition state all favor a tighter variational transition state, whereas only one of the other four modes favors a tighter transition state. The canonical variational transition state for OH + H_2S is at -0.038 Å at 300 K, at -0.025 Å at 800 K, and at $+0.069$ Å at 2400 K.

The difference between CVT and CVT/SCT at 2400 K is from the CVT/CAG transmission coefficient discussed above. This is not necessarily reliable at high-temperature (because it is based on the ground state), so it might be more accurate to accept the CVT prediction at high temperature.

Conclusions

The reaction of OH with H_2S has proved to be a difficult reaction to model. Lafage et al.[9] concluded that the temperature dependence is difficult to interpret if the reaction is a simple abstraction reaction. In the present study we show, however, that this temperature dependence can be accounted for even in the context of a simple abstraction reaction. Rate constants have been calculated with the M06-2X/MG3S method, the RPG treatment of the multiple-well torsional mode, and a proper consideration of symmetry, and they are in good agreement with published experimental results. A negative classical barrier height has been found, but there is a positive maximum of 0.25 kcal/mol in the vibrationally adiabatic ground-state potential-energy curve (which is the same as the generalized free energy of activation profile in the low-temperature limit). The success of the new density functional in explaining this reaction apparently results from achieving the proper balance between attractive noncovalent interactions and the activation cost of the bond rearrangement. A correct treatment of the nonsuperimposable mirror images at the transition state is also essential to modeling this reaction.

Acknowledgment. This work was supported in part by the U.S. Department of Energy, Office of Basic Energy Sciences, by Grant No. DOE-FG02-86ER13579.

Supporting Information Available: Complete refs 15 and 25, a table of TST, CVT, and CVT/SCG rate constants at 13 temperatures, a table of CVT/CAG contributions to the transmission coefficient, and the absolute energies (in hartrees) and optimized geometries (as Cartesian coordinates) of all calculated structures. This material is available free of charge via the Internet at http://pubs.acs.org.

JA072538B